AGU PUBLICATIONS

Geophysical Research Letters

RESEARCH LETTER
10.1002/2016GL070150

Key Points:
- Isotopic forward model is developed for tropical ice cores based on Quelccaya Ice Cap observations
- Quelccaya snow isotopic seasonality stems from progressive monsoon depletion and winter enrichment
- Including synoptic event amount effect fractionation improves annual isotope profile simulation

Supporting Information:
- Supporting Information S1

Correspondence to:
J. V. Hurley,
jvhurley12@gmail.com

Citation:
Hurley, J. V., M. Vuille, and D. R. Hardy (2016), Forward modeling of δ^{18}O in Andean ice cores, *Geophys. Res. Lett.*, *43*, doi:10.1002/2016GL070150.

Received 22 JUN 2016
Accepted 19 JUL 2016
Accepted article online 23 JUL 2016
Corrected 15 AUG 2016

This article was corrected on 15 AUG 2016. See the end of the full text for details.

Forward modeling of δ^{18}O in Andean ice cores

J. V. Hurley[1], M. Vuille[1], and D. R. Hardy[2]

[1]Department of Atmospheric and Environmental Sciences, State University of New York at Albany, Albany, New York, USA, [2]Department of Geosciences, University of Massachusetts Amherst, Amherst, Massachusetts, USA

Abstract Tropical ice core archives are among the best dated and highest resolution from the tropics, but a thorough understanding of processes that shape their isotope signature as well as the simulation of observed variability remain incomplete. To address this, we develop a tropical Andean ice core isotope forward model from in situ hydrologic observations and satellite water vapor isotope measurements. A control simulation of snow δ^{18}O captures the mean and seasonal trend but underestimates the observed intraseasonal variability. The simulation of observed variability is improved by including amount effects associated with South American cold air incursions, linking synoptic-scale disturbances and monsoon dynamics to tropical ice core δ^{18}O. The forward model was calibrated with and run under present-day conditions but can also be driven with past climate forcings to reconstruct paleomonsoon variability. The model is transferable and may be used to render a (paleo)climatic context at other ice core locations.

1. Introduction

Stable water isotopes (δD and δ^{18}O) embedded in tropical ice cores and other archives are among the most important proxies used for paleoclimate reconstruction on a variety of time scales, but their climatic interpretation often remains controversial [*Bradley et al.*, 2003; *Hoffman et al.*, 2003; *Vimeux et al.*, 2009; *Vuille et al.*, 2012; *Thompson et al.*, 2013]. Isotope-enabled climate models and satellite measurements of isotope ratios in water vapor yield simulated and observational isotopic values that can be compared directly with these isotopic proxies, without the need for an often error-prone conversion into temperature or precipitation amount [e.g., *Vuille et al.*, 2003a]. Such errors may arise from age model uncertainty or incomplete understanding of the climate-proxy system [*Sachs et al.*, 1977; *Tingley et al.*, 2012; *Evans et al.*, 2013; *Dee et al.*, 2015]. Direct comparisons between isotopic proxies and both isotope-enabled models and satellite measurements, however, do not consider the proxy-dependent fractionations or postdepositional alterations that might affect the isotopic composition in each proxy archive. There may also be downscaling issues related to comparison of large-grid general circulation model simulations and single proxy sites which potentially record local or microclimate signals. Isotopic forward models are therefore increasingly being developed to allow for a more accurate simulation of how proxies incorporate and store isotopic information [e.g., *Sturm et al.*, 2010; *Thompson et al.*, 2011; *Tierney et al.*, 2011; *Baker et al.*, 2012; *Brönnimann et al.*, 2012; *Evans et al.*, 2013; *Dee et al.*, 2015].

Here we develop a forward model for high-resolution ice core isotope records from tropical Andean glaciers with high accumulation rates. These records are fundamental to our understanding of tropical climate dynamics on human timescales. Our forward model is developed using a decade of observations from both field campaigns and an Automated Weather Station (AWS) installed on the summit of Quelccaya Ice Cap in the Peruvian Andes. This retreating ice cap is home to one of the most important records of tropical paleoclimate for the last 1800 years [*Thompson et al.*, 1985, 2013; *Chadwell et al.*, 2016]. Variability of precipitation and isotope ratios at Quelccaya has been linked to Intertropical Convergence Zone (ITCZ) variability and precipitation, El Niño–Southern Oscillation (ENSO), and South American Summer Monsoon (SASM) intensity [*Thompson et al.*, 1985, 1993; *Vuille and Werner*, 2005; *Vuille et al.*, 2012]. Pacific equatorial sea surface temperatures (SSTs) have also been linked to Quelccaya isotope ratios, both directly [*Vuille et al.*, 2003b; *Thompson et al.*, 2013] and by applying intermediate complexity proxy system model (PSM) simulations [*Dee et al.*, 2015]. However, both forward modeling and isotope-enabled general circulation model (GCM) modeling efforts have failed to fully capture (and indeed, significantly underestimate) the observed variability in Quelccaya isotope ratios [*Tindall et al.*, 2009; *Dee et al.*, 2015]. Here we present a mechanistic forward model based on the local hydrologic cycle to simulate Andean snow oxygen isotope ratios and show that such a model is capable of accurately simulating intraseasonal, seasonal, and interannual variability of δ^{18}O. The *delta* notation is an

expression of a sample's isotope ratio in parts per thousand or *per mil*(‰), normalized by the isotope ratio of the standard

$$\delta = \left(\frac{R_{\text{sample}}}{R_{\text{std}}} - 1 \right) \times 1000. \quad (1)$$

The oxygen isotope ratios (δ^{18}O) in snow from the summit of Quelccaya are lowest during austral summer (~24 ‰) and highest in austral winter (~17‰), in a pattern opposite to the seasonal temperature cycle [*Thompson and Dansgaard*, 1975; *Thompson*, 1980]. In the absence of a simple temperature control, the inverted seasonal δ^{18}O cycle at Quelccaya has long been considered a product of atmospheric circulation [*Thompson*, 1980], upstream processes [*Vuille et al.*, 2012; *Samuels-Crow et al.*, 2014], and the amount effect [*Dansgaard*, 1964; *Rozanski et al.*, 1993]. The amount effect describes the inverse empirical relationship between δ values and tropical precipitation amount and has been shown to arise principally as a consequence of reevaporation and recycling during convection [*Risi et al.*, 2008]. Austral summer convection over the Amazon Basin preferentially removes the heavier isotopes of oxygen and hydrogen during intense precipitation events as vapor is transported from the tropical Atlantic to the western Amazon Basin [*Hoffman et al.*, 2003]. Consequently, summer vapor δ values from the western Amazon Basin are observed to be lower than δ values from the source region over the tropical western Atlantic. In contrast, when convection over the Amazon Basin is suppressed in austral winter (June–August, JJA), water vapor δ values from the western Amazon Basin (6° box centered at 69°W, 11°S) are observed to be comparable to those from the vapor source over the tropical western Atlantic (6° box centered at 42°W, 1°S) (Figures 1a and 1b). This reflects dynamic easterly transport of vapor across the Amazon Basin from the Atlantic to the Andes without reduction of the isotope ratios such as occurs during summer. The seasonality of western Amazon Basin water vapor δ values (Figure 1b), together with the seasonality of snow accumulation at the summit of Quelccaya (Figure 1c), yields a climatology of the water isotopologue ratios in snow that is indicative of SASM activity over the western Amazon Basin (Figure 1d).

Grootes et al. [1989] were the first to use water isotopologue and water vapor mass balance calculations to explain the seasonality of snow δ^{18}O at the summit of Quelccaya as a sum of (i) enhanced summer convection and fractionation over the Amazon Basin; (ii) seasonally similar Rayleigh fractionation up to the altitude of Quelccaya; and (iii) postdepositional enrichment, enhanced during winter, at the surface of the Ice Cap. *Stichler et al.* [2001] described postdepositional δ alteration using a sublimation mass loss model for surface snow atop a high-altitude subtropical Andean glacier. Sublimation between snowfall events and during the dry season (i) leads to mass loss of snow and (ii) raises values of surface snow δ^{18}O and δD [*Stichler et al.*, 2001]. Here we follow the work of *Grootes et al.* [1989] and *Stichler et al.* [2001] to propose a new tropical ice core forward model simulating annual snow layer δ^{18}O profiles at the summit of Quelccaya. We augment and merge the approaches described in these two studies with (i) an observational data set compiled from monitoring activities at the summit of Quelccaya over the past decade and (ii) satellite observations of water vapor isotopologues over Quelccaya and the Amazon Basin. The novelty of this study lies in (i) the development of a forward model capable of simulating not only the seasonal [*Grootes et al.*, 1989] but also the intraseasonal and interannual variability of snow δ^{18}O, (ii) its transferability to other ice core sites, and (iii) its suitability for a wide range of paleoclimatic applications.

Our forward model builds upon prior PSMs developed to simulate Alpine ice core [*Brönnimann et al.*, 2012] and specifically Quelccaya δ^{18}O [*Dee et al.*, 2015]. By restricting our analyses to the recent decade of snowfall, we sidestep the need to explicitly model compaction [*Li and Zwally*, 2011] and diffusion [*Gkinis et al.*, 2014; *van der Wel et al.*, 2015]; such as would be necessary for simulation of the full Quelccaya proxy archive [*Dee et al.*, 2015]. Rather, as a distinct contribution to proxy system modeling, we explore how the hydrologic cycle elements of ablation and sublimation influence the recording of δ^{18}O in the ice sensor [*Evans et al.*, 2013], where the sensor receives the climate signal that is recorded in the archive. We also test the sensitivity of isotope ratios of snow to (i) variations in initial convective vapor height, (ii) the rate and depth of sublimation, and (iii) the amplitude of the amount effect.

We recently established that up to 70% of the snowfall at Quelccaya is triggered by South American cold air incursions [*Hurley et al.*, 2015]. These events are a response to interactions between midlatitude westerlies, topography of the Andes, and southerly advection of extratropical air with low moist static energy (MSE) [*Garreaud and Wallace*, 1998; *Garreaud*, 1999, 2000, 2001]. Downstream amplification of an extratropical

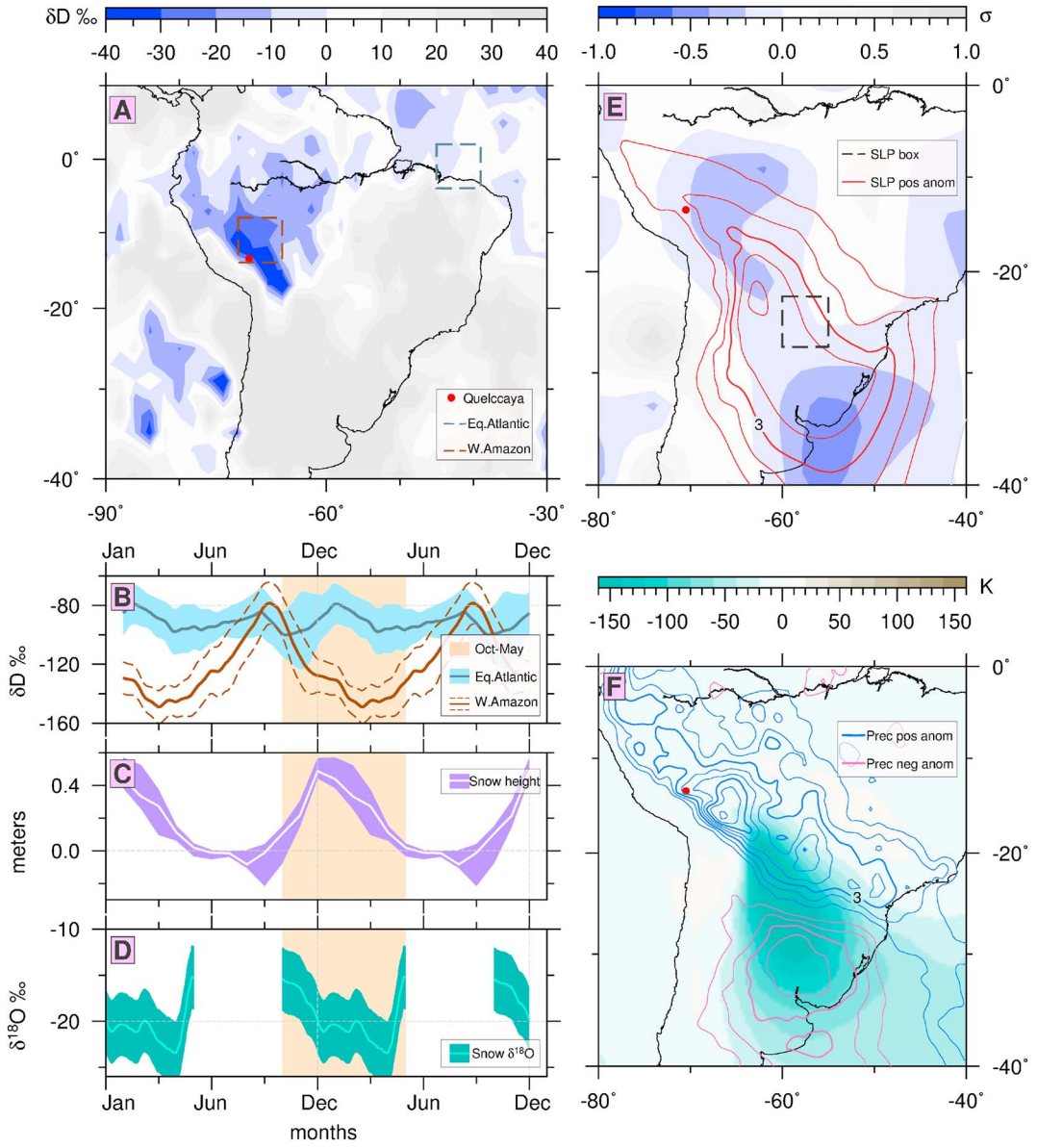

Figure 1. (a) TES lower troposphere (750 hPa) water vapor δD seasonality, DJF minus JJA (2004–2012). Red circle indicates location of Quelccaya Ice Cap, Peru. (b) Seasonal cycle of lower troposphere water vapor δD, from source over the equatorial Atlantic (blue lines, blue box in Figure 1a) and western Amazon Basin (brown lines, brown box in Figure 1a). Solid lines are mean values. Shading and dashed lines indicate the mean $\pm$ 1 standard deviation. (c) Net monthly snow accumulation at Quelccaya summit, median (solid white curve) and 25th–75th quantile envelope from the interannual distribution of values (purple shading, 2004–2014 from *Hurley et al.* [2015]). (d) Snowfall δ^{18}O as a function of month, mean (solid light green curve), and 1 standard deviation envelope (green shading), from snowpits at the summit of Quelccaya (2004–2005, 2005–2006, 2006–2007, 2007–2008, 2008–2009, 2010–2011, and 2013–2014). Beige shading (Figures 1b–1d) highlights monsoon season October–April. (e) Normalized DJF cold air incursion composite anomalies of water vapor δD (σ, shading) and sea level pressure (contours, red positive, 1 hPa interval). Black dash box represents area over which cold air incursions are identified from the area-average sea level pressure. (f) DJF cold air incursion composite anomalies of eddy meridional transport of moist static energy (shading, K m s^{-1} — no positive values within field of view) and precipitation (contours, blue positive, pink negative, 0 contour omitted, and contour interval 1 mm day^{-1}).

cyclone over the South Atlantic coincides with advance of an anticyclone around and over the southern Andes into southern South America (Figure 1e). Southerly wind anomalies on the west side of the extratropical cyclone advect the surface high-pressure system and low-troposphere cold and dry air northwestward across the continent [*Müller et al.*, 2015]. As the cold front progresses to lower latitudes, available moisture increases and convection strengthens, resulting in a positive precipitation anomaly from the Rio de la Plata basin to the western Amazon Basin (Figure 1f).

Given the relevance of cold air incursions for snowfall generation on Quelccaya [*Hurley et al.*, 2015] we incorporate incursions as super-Rayleigh fractionation events into our forward model of Andean snow $\delta^{18}O$. We hypothesize that inclusion of such events will improve the simulation of these salient tropical proxy archives and allow us to link them to SASM dynamics.

2. Data and Methods

The AWS has been continuously operating since 2004 at 5680 m altitude on the summit of Quelccaya (70.82°W, 13.93°S), collecting daily in situ meteorological observations of accumulation and ablation [*Hurley et al.*, 2015]. Snow height is measured acoustically by two identical instruments mounted on the system tower, recording the distance between the sensor and the surface of the snow. Accuracy for hourly snow height measurements is about ±0.01 m. In the development of the forward model, we rely on a daily product of snow height change, condensed from the dual-instrument hourly observations through 2014 to accurately constrain the local hydrologic cycle.

For comparison with observations, we evaluate our simulated snow $\delta^{18}O$ profiles against measured values from eight snowpits covering the following hydrologic years (June–May): 2004–2005, 2005–2006, 2006–2007, 2007–2008, 2008–2009, 2010–2011, and 2013–2014. The 2013–2014 was sampled twice, both in April at the end of the wet season and again in October at the end of the dry season.

We use satellite observations of water vapor HDO $[H_2O]^{-1}$ ratios from the Tropospheric Emission Spectrometer (TES), which is a thermal infrared spectrometer aboard the National Aeronautics and Space Administration's Aura satellite [*Worden et al.*, 2006]. We use the bias-corrected level 2 version 6 Lite Product HDO and H_2O products (L2v005_litev08) [*Worden et al.*, 2011, 2012; *NASA*, 2015].

For information on both the thermal structure of the atmosphere and sea level pressure, required to identify South American cold air incursions, we use 0.7° four times daily surface and pressure level data from the ERA-Interim reanalysis [*Dee et al.*, 2011].

Our forward model to simulate $\delta^{18}O$ values at the summit of Quelccaya (Figure 2a) is driven by daily observations of snow height change (Figure 2b). On days of snow height gain, $\delta^{18}O$ of fresh snowfall is simulated as a product of Rayleigh condensate fractionation (Figures 2c and 2d). Between snow height gain events, and during periods of suppressed convection (such as during austral winter), the near-surface snow $\delta^{18}O$ profile is modified by both sublimation and mass loss. This effectively raises near-surface δ values and lowers the snow surface height, particularly during austral winter.

We first complete a control (CTRL) simulation based on AWS and TES observations and reanalysis data. To assess the usefulness of the forward model when driven with GCM output, we then complete a control simulation where we substitute isotope-enabled GCM output for TES observations and reanalysis data. To do this, we use the multimodel average of monthly water vapor isotope and temperature output from the Stable Water Isotope Intercomparison Group, Phase 2 (SWING2) [*Risi et al.*, 2012] (Table S1 in the supporting information).

To estimate daily snowfall δ values, we developed a daily isotope climatology from Rayleigh fractionation models (Figures 3c and 3d). Initial vapor δ values are based on TES observations of lower troposphere (750 hPa) water vapor isotopologues over the western Amazon Basin (Figure 1b, brown curve). Rayleigh models were developed using the familiar equation

$$\ln\left(\frac{R}{R_o}\right) = (\alpha - 1)\ln\left(\frac{q}{q_o}\right), \tag{2}$$

where R is the abundance ratio of heavy to light isotope, the o subscript refers to initial values, α is the equilibrium fractionation factor, and q is the water vapor mixing ratio. Rayleigh distillation is simulated to proceed from the initial conditions of δD_o, T_o and q_o of the lower troposphere to the upper troposphere

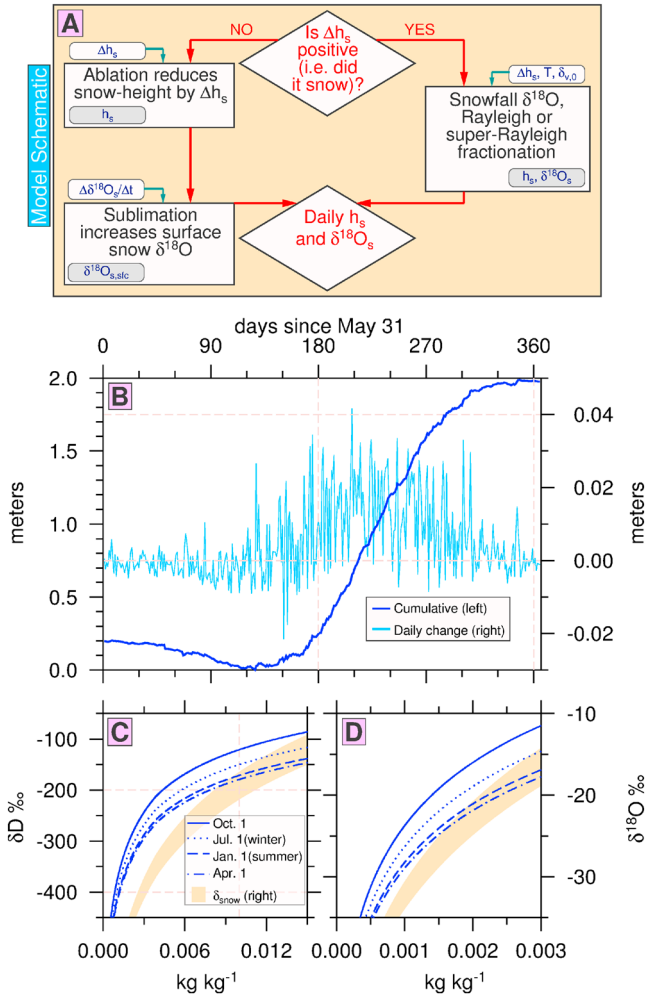

Figure 2. Model description. (a) Snow $\delta^{18}O$ forward model diagram for daily solution. Red arrows indicate process flow through the model. Square boxes contain modules. Input (no shading) and output (gray shading) for modules shown by rounded boxes. Flow into modules is indicated by cyan arrows. Δh_s, change in snow height; h_s, snow height; $\Delta\delta^{18}O_s/\Delta t$, enrichment rate; $\delta^{18}O_{s,sfc}$, surface snow isotope ratio; T, temperature; $\delta_{v,0}$, initial vapor isotope ratio; and $\delta^{18}O_s$, snow isotope ratio. (b) Time-mean (2003–2014) seasonal cycle (June–May) of AWS daily snow height change at the summit of Quelccaya. The dark blue curve (left axis) represents cumulative sum of daily snow height change. Light blue curve (right axis) indicates daily change in snow height. (c) Seasonal distribution of Rayleigh model water vapor δD (per mil, ‰); versus mixing ratio, q (x axis); 1 January, dashed; 1 April, dash dotted; 1 July, dotted; and 1 October, solid. Beige shading indicates seasonal distribution of q versus δD values for super-Rayleigh fractionation. (d) As Figure 1c but for $\delta^{18}O$ of snow.

above Quelccaya. We use the daily climatology of ERA-Interim temperature profiles over the western Amazon Basin (brown box in Figure 1a). At upper troposphere temperatures below 263 K, α is replaced by a fractionation factor that includes kinetic effects [*Ciais and Jouzel*, 1994],

$$\alpha_{\text{ice}}^{\text{eff}} = (\alpha S)\left(1 + \alpha[S-1]\frac{D}{D_{\text{iso}}}\right)^{-1}. \tag{3}$$

Following *Bony et al.* [2008], we use diffusivities for the light and heavy isotopes (D and D_{iso}) described in *Merlivat* [1978], and S is the supersaturation with respect to ice. To simulate super-Rayleigh distillation associated with intense synoptic systems, we implement the fractionation factor parameterization of *Noone* [2012]

$$\alpha_p = \alpha(1+\phi), \tag{4}$$

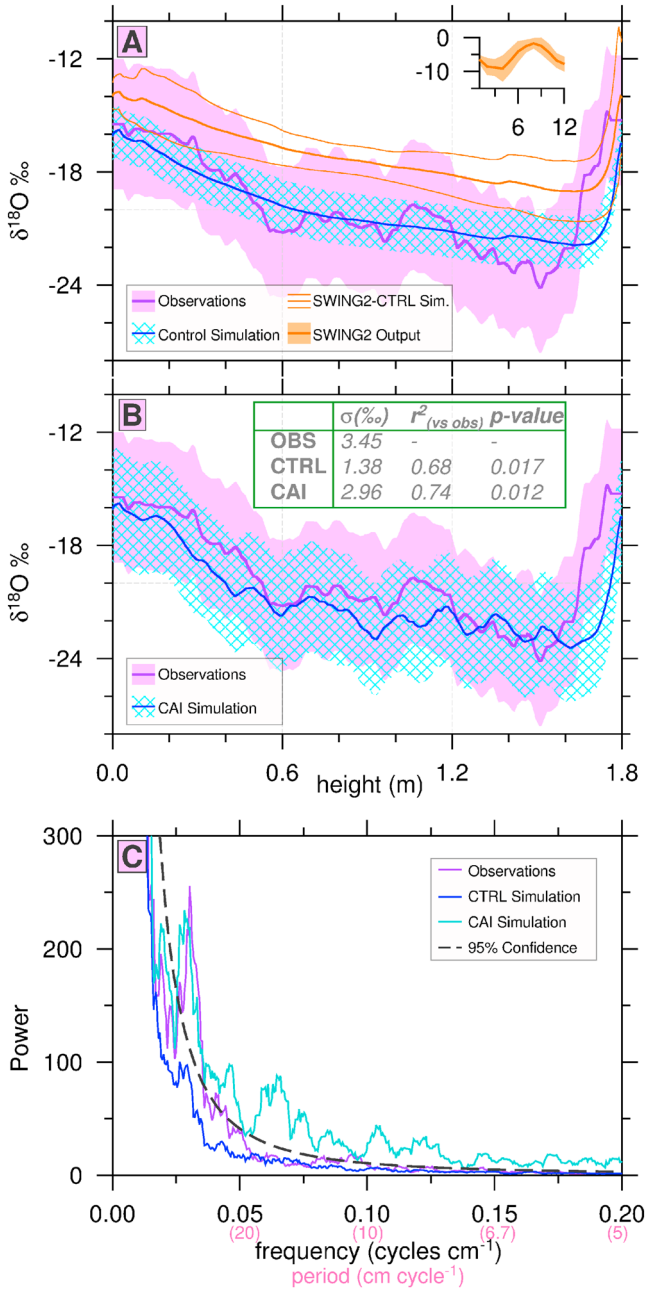

Figure 3. (a) Control simulation of snow $\delta^{18}O$ profile ($\delta^{18}O$ versus height above the base of snow layer, solid blue curve) ± 1 standard deviation (σ blue hachure pattern), compared with observed snow $\delta^{18}O$ profile, mean (μ solid magenta curve), ± 1 σ (magenta shading). CTRL simulation using SWING2 data (orange; μ thick curve, ± 1 σ thin curves). Inset shows SWING2 climatology (x axis months, 6 = June) for Quelccaya precipitation $\delta^{18}O$ (multimodel μ orange curve, ± 1 σ orange shading). (b) As in Figure 3a but with super-Rayleigh fractionation on cold air incursion days. Inset table summarizes statistics for observed profile (OBS), the control simulation (CTRL), and the cold air incursion simulation (CAI); standard deviation (σ), r^2 values of simulated versus observed $\delta^{18}O$, and corresponding p values. (c) Snow $\delta^{18}O$ periodograms (2003–2014, power versus frequencies (cycles cm^{-1}); periods indicated by pink x axis labels) for OBS (magenta), CTRL (blue), and CAI (cyan). Dashed black line indicates 95% confidence red noise spectrum from 10,000 Monte Carlo simulations. The spectra for both OBS and the CAI simulation exhibit a significant peak at a period of about 33 cm $cycle^{-1}$.

where α_p is the parameterized super-Rayleigh fractionation factor, α is the nonparameterized fractionation factor, and ϕ is an approximation of the departure from equilibrium. As in *Noone* [2012], we use ϕ=0.1. Fractionation under super-Rayleigh conditions leads to a condensate, as well as a residual vapor, with δ values lower than those produced by equilibrium fractionation, as depicted by the beige areas in Figures 2c and 2d. To approximate cold air incursion amount effects, precipitation δ values for these events are simulated by super-Rayleigh distillation models and the fractionation factor parameterization. This is done in a separate cold air incursion (CAI) simulation of δ^{18}O.

To simulate the increase of near-surface snow δ values by means of sublimation, we estimate a daily rate of enrichment or isotope ratio increase following *Stichler et al.* [2001]. Details of sublimation and enrichment calculations are summarized in the supporting information (Text S1 and Figure S1). To calculate the enrichment rate, we first approximate the sublimation rate v ~0.006 m d^{-1} using Quelccaya summit snowpit measurements over the past decade (Figure S1). From v we then estimate the daily modification of near-surface snow δ^{18}O to be ~0.8‰ d^{-1}. These estimates of both sublimation and enrichment rates for Quelccaya are consistent with previous studies. *Stichler et al.* [2001] found v to be ~0.01 m d^{-1} and an enrichment rate of 0.7‰ d^{-1} at Cerro Tapado glacier, a high-altitude subtropical Andean glacier. *Grootes et al.* [1989] determined the enrichment rate at Quelccaya in 1983 to be approximately 0.5‰ d^{-1}. In our forward model, we increase the δ^{18}O values of snow in the top 0.1 m by 0.8‰ on days of snow height loss. *Stichler et al.* [2001] estimated the sublimation depth at Cerro Tapado to be about 0.05–0.10 m, and *Grootes et al.* [1989] estimated enrichment to occur to depths of about 0.05–0.20 m. The enrichment depth and rate used here are consistent with the observation that on average, postdepositional modification of Quelccaya snowpit δ^{18}O values is limited to about the top 0.2–0.3 m.

To complete the CAI simulation, we first identify South American cold air incursion events from the ERA-Interim reanalysis, following the approach of *Garreaud* [2000]. This is based on evaluation of the daily sea level pressure (SLP) tendency, or daily change, averaged over a 5° by 5° box (Figure 1e) centered on 25°S, 57.5°W. Cold air incursions were identified as events where the SLP tendency is within the top 10% of the seasonal frequency distribution and the daily SLP magnitude is greater than or equal to the seasonal median [*Garreaud*, 2000]. Incursions identified in this way from the ERA-Interim reanalysis (2003–2014) have composite structures that correspond with previous investigations (Figures 1e and 1f) [*Garreaud*, 2000, 2001; *Hurley et al.*, 2015].

For the CAI simulation of Quelccaya snow δ^{18}O, we model snowfall on cold air incursion days as a product of super-Rayleigh fractionation, as discussed above. In this way, we simulate the amount effect or depletion of heavy isotopes during these intense precipitation events. TES water vapor δD over the western Amazon Basin is lower on cold air incursion days compared to the seasonal average (Figure 1e, shading). This is consistent with observations of anomalously low water vapor δ values on the Chajnantor Plateau in the Andes of northern Chile during incursion events [*Galewsky*, 2015]. These observations are integrated into the CAI simulation via the use of lower initial vapor δ values on cold air incursion days (Figures 2c and 2d, shading). For incursion days, we use an initial vapor δD value equal to the 2003–2014 daily mean value minus 1 standard deviation (Figure 1b, lower dashed brown line), which corresponds to a reduction of approximately 10‰.

Sensitivity analyses were conducted to evaluate how the forward model responds to variations in the initial vapor height, sublimation enrichment rate and depth, and the degree to which amount effects deviate from equilibrium. The results of these sensitivity tests are given in Text S2–S4.

In reference to recent nomenclature for forward model design and complexity choices, the ice core forward model presented here is a high-complexity model [*Evans et al.*, 2013; *Dee et al.*, 2015] as it uses site-specific information. This is in contrast to the isotope-enabled GCMs [*Sturm et al.*, 2010; *Sjolte et al.*, 2011; *Steen-Larsen et al.*, 2011] or the intermediate complexity ice core PSM model used within the PRoxY System Modeling (PRYSM) framework [*Dee et al.*, 2015].

3. Results

The CTRL-simulated snow δ^{18}O profile accurately simulates the observed mean values, seasonality, and tendency toward more negative values through the austral summer on the summit of Quelccaya (Figure 3a). However, it does not capture the magnitude of the observed intraseasonal variability nor capture the interannual variability as expressed by the much larger standard deviation of the observations. The simulated δ^{18}O

profile suggests that initializing the CTRL simulation with TES water vapor δ values and synoptic-scale perturbations of upper troposphere temperature above Quelccaya is insufficient to account for the observed intraseasonal and interannual variability of snow δ^{18}O at Quelccaya. We show below that inclusion of amount effects associated with cold air incursions facilitates simulation of the observed δ^{18}O variability.

Substituting observations with SWING2 isotope-enabled GCM output yields a δ^{18}O profile which is qualitatively similar (Figure 3a, orange curves), though δ^{18}O values are about 2‰ higher than observations and the CTRL simulation. However, this SWING2-CTRL simulation nonetheless results in an estimate of Quelccaya snow δ^{18}O that is a clear improvement when compared with the direct SWING2 model output of precipitation δ^{18}O near Quelccaya (Figure 3a, inset). This illustrates the usefulness of the forward model for capturing proxy-specific processes which enhance the isotopic variability at the site.

Further, if we consider lower or higher initial vapor starting heights (824 and 681 hPa) for the Rayleigh models, the mean value of the simulated snow δ profile correspondingly increases or decreases (Figure S2). However, the intraseasonal pattern of snow δ^{18}O does not vary in response to the initial height in the Rayleigh model.

Sublimation principally influences δ values near the top and bottom of the annual profile (Figure S3), representing periods with longer dry spells at the onset and end of the wet season, respectively. Postdepositional modification of near-surface snow δ values is, however, insufficient to account for the 2–4‰ amplitude of observed intraseasonal variability during the core of the wet season. This is not surprising given that dry spells during the wet season, when enrichment due to sublimation could play an important role, are rare (Figure 2b). Instead, our results suggest that intraseasonal δ^{18}O variability during the core wet season is fundamentally a result of variations in snowfall δ values.

We next model snowfall δ^{18}O of midlatitude cold air incursions as a product of super-Rayleigh fractionation (Figure 3b). δ^{18}O from the CAI simulation explains 74% ($p = 0.012$) of the observed variance, compared with 68% ($p = 0.017$) for the CTRL simulation. Simulation of interannual δ^{18}O variability is also improved as indicated by the profile-average standard deviation (σ) of the CAI simulation which increases to 2.96‰ from 1.38‰ for the CTRL simulation ($\sigma_{observed}$=3.45‰). In the frequency domain and in comparison with a first-order autoregressive (AR1) process (Figure 3c), the CAI simulation shares a significant peak with the observations corresponding to intraseasonal periods of about 33 cm cycle^{-1} (corresponding to about 3 weeks in the wet season). The peak is not significant in the CTRL simulation, suggesting that it is related to synoptic-scale amount effects and the large-scale circulation.

Finally, the degree to which fractionation deviates from equilibrium directly corresponds to the amplitude of the simulated intraseasonal variability (Figure S4). This suggest that extratropical cold air incursions may be responsible for much of the intraseasonal variability seen in the ice core δ^{18}O from Quelccaya.

Our results highlight how monsoon dynamics and synoptic disturbances are encoded in Andean tropical ice core isotope records. This connection between δ^{18}O variability and climate dynamics suggests that the ice core archives may be used to reconstruct the paleoclimate of the SASM.

4. Discussion and Conclusion

We have developed an isotope forward model for the annual snow δ^{18}O profile at the summit of the Quelccaya Ice Cap, driven by a daily record of snow height change and based, in part, on satellite observations of water vapor stable isotopologue ratios. In the CTRL simulation we model snowfall at Quelccaya as a product solely of Rayleigh fractionation from a daily climatology of initial vapor δ values that are consistent with TES observations of the lower troposphere over the western Amazon Basin. In doing so, we are able to simulate (r=0.82) the observed seasonality of Quelccaya snow δ^{18}O as a function of austral summer convection and preferential removal of the heavier isotope over the Amazon Basin. However, the CTRL simulation underestimates the observed amplitude of intraseasonal variability and interannual standard deviation of δ^{18}O values. When including the influence of midlatitude cold air incursions by simulating related snowfall δ^{18}O as a product of super-Rayleigh fractionation from a vapor with a lower initial δ value, the correlation between observed and simulated δ^{18}O profiles increases, the difference between observed and simulated interannual δ^{18}O standard deviation decreases, and the power spectrum of the simulated δ^{18}O shares a significant intraseasonal periodicity with the observations.

The findings of this study link synoptic-scale climate dynamics to variability of a tropical Andean ice core δ^{18}O archive, indicating a potential for using such archives to reconstruct the history of the SASM. Synoptic-scale

variability is recorded in tropical ice core $\delta^{18}O$ as the isotope signature is inherited from snow that falls during storm events. In this way, ice core $\delta^{18}O$ archives may record some measure of interannual synoptic-scale disturbance variability. Tropical Andean $\delta^{18}O$ is also correlated to SSTs [*Thompson et al.*, 2013], and so it is intriguing to consider how equatorial Pacific SSTs may force cold air incursion activity [*Diaz et al.*, 1998; *Gonçalves et al.*, 2002]. Reconstruction of the SASM history and future monitoring and modeling of Quelccaya $\delta^{18}O$ over the past millenium are subjects of ongoing studies by the authors.

There are shortcomings to the model presented here. It does not account for compaction and diffusion [*Dee et al.*, 2015] as would be necessary for simulating the 1800 year archive. The simulations appear to underestimate the depth to which sublimation alters near-surface snow δ values. The influence of both initial Rayleigh model height and sublimation enrichment depth and rate is explored in the supporting information. By holding these parameters constant in the CTRL and CAI simulations, we simplify interpretation of the influence of synoptic-scale variability. However, most of the snowfall at Quelccaya is a product of cold air incursions, and so it is physically meaningful to simulate the synoptic-scale variability as presented here. Furthermore, Quelccaya upper troposphere vapor δ values during cold air incursions are lower than would be expected by a Rayleigh model [*Hurley et al.*, 2015], linking cold air incursions to super-Rayleigh fractionation.

Our simulations confirm the role played by the seasonal monsoon progression in priming δ values over the western Amazon Basin and forcing the seasonal reduction of isotope ratios seen in the Quelccaya snow throughout the wet season. Sublimation-related increase of near-surface snow isotope ratios during the dry season is required to accurately simulate the annual snow $\delta^{18}O$ profile at Quelccaya.

The forward model presented here can readily be applied at other tropical ice core locations. Our high-complexity model solves for daily changes in snow height and isotope ratios, as we had monitoring data and daily in situ observations available. In the absence of such data, climatologies of the hydrologic cycle, temperature, and water vapor isotope ratios could be used to drive the conceptual model on a monthly time step, thereby placing the proxy record in a climatic framework.

Looking forward, we intend to drive our model with GCM output for the last millenium, such as from the Paleoclimate Modelling Intercomparison Project III (PMIP3). Most PMIP3 models are not isotope-enabled (although see *Colose et al.* [2016]), and we expect to solve for western Amazon Basin vapor δ values by way of offline calculations. As more isotope-enabled and intermediate complexity last millenium simulations [*Dee et al.*, 2014] become available this work can be expanded. Combining GCM output for the last millenium with our forward model will allow us to assess the role of various forcings (solar, volcanic, and land use) in shaping decadal to centennial-scale variability as tracked by high-resolution ice core records. This will also allow us to evaluate if and how past changes in cold air incursion intensity or frequency may have left an imprint in the Quelccaya ice core $\delta^{18}O$ record, which has implications for proxy system modeling, climate dynamics, and paleoclimate of the SASM.

Acknowledgments

The authors thank Sylvia Dee and one anonymous reviewer whose comments vastly improved the quality of this paper. ERA-Interim reanalysis was obtained from the Research Data Archive (RDA) that is maintained by the Computational and Information Systems Laboratory at the National Center for Atmospheric Research (NCAR). NCAR is sponsored by the National Science Foundation (NSF). The original data are available from the RDA (http://rda.ucar.edu) in data set number ds627.0. GPCP 1 daily precipitation data were obtained from the NASA Goddard Space Flight Center (http://precip.gsfc.nasa.gov). TES Lite Products data were obtained from the NASA Jet Propulsion Laboratory (tes.jpl.nasa.gov/data/). The authors gratefully acknowledge the financial support from NSF-P2C2 (AGS-1303828), NSF Paleoclimate (9909201 and 0402557), and the NOAA Global Climate Observing System. Data and model code unique to this study may be obtained upon request from the authors.

References

Baker, A., C. Bradley, S. Phipps, M. Fischer, I. Fairchild, L. Fuller, C. Spötl, and C. Azcurra (2012), Millennial-length forward models and pseudoproxies of stalagmite $\delta^{18}O$: An example from NW Scotland, *Clim. Past*, *83*(4), 1153–1167.

Bony, S., C. Risi, and F. Vimeux (2008), Influence of convective processes on the isotopic composition ($\delta^{18}O$ and δD) of precipitation and water vapor in the tropics: 1. Radiative-convective equilibrium and Tropical Ocean-Global Atmosphere-Coupled Ocean-Atmosphere Response Experiment (TOGA-COARE) simulations, *J. Geophys. Res.*, *113*, D19305, doi:10.1029/2008JD009942.

Bradley, R. S., M. Vuille, D. R. Hardy, and L. G. Thompson (2003), Low latitude ice cores record Pacific sea surface temperature, *Geophys. Res. Lett.*, *40*(4), 1174, doi:10.1029/2002GL016546.

Brönnimann, S., I. Mariani, M. Schwikowski, R. Auchmann, and A. Eichler (2012), Simulating the temperature and precipitation signal in an Alpine ice core, *Clim. Past Discuss.*, *8*, 6111–6134.

Chadwell, C. D., D. R. Hardy, C. Braun, H. H. Brecher, and L. G. Thompson (2016), Thinning of the Quelccaya Ice Cap over the last thirty years, *Cryosphere Discuss.*, doi:10.5194/tc-2016-40, in press.

Ciais, P., and J. Jouzel (1994), Deuterium and oxygen 18 in precipitation: Isotopic model, including mixed cloud processes, *J. Geophys. Res.*, *99*, 16,793–16,803.

Colose, C. M., A. N. LeGrande, and M. Vuille (2016), The influence of volcanic eruptions on the climate of tropical South America during the last millenium in an isotope-enabled general circulation model, *Clim. Past*, *12*, 961–979.

Dansgaard, W. (1964), Stable isotope in precipitation, *Tellus*, *16*, 436–468.

Dee, D. P., et al. (2011), The ERA-Interim reanalysis: Configuration and performance of the data assimilation system, *Q. J. R. Meteorol. Soc.*, *137*, 553–597.

Dee, S., D. Noone, N. Buenning, J. Emile-Geay, and Y. Zhou (2014), SPEEDY-IER: A fast atmospheric GCM with water isotope physics, *J. Geophys. Res. Atmos.*, *120*, 73–91, doi:10.1002/2014JD022194.

Dee, S., J. Emile-Geay, M. N. Evans, A. Allam, E. J. Steig, and D. M. Thompson (2015), PRYSM: A open-source framework for PRoxY System Modeling with applications to oxygen- isotope systems, *J. Adv. Model. Earth Syst.*, *7*, 1220–1247, doi:10.1002/2015MS000447.

Diaz, A. F., C. D. Studzinski, and C. R. Mechoso (1998), Relationships between precipitation anomalies in Uruguay and southern Brazil and sea surface temperature in the Pacific and Atlantic Oceans, *J. Clim.*, *11*, 251–271.

Evans, M., S. Tolwinski-Ward, D. Thompson, and K. Anchukaitis (2013), Application of proxy system modeling in high resolution paleoclimatology, *Quat. Sci. Rev.*, *76*, 16–28.

Galewsky, J. (2015), Constraining supersaturation and transport processes in a South American cold-air outbreak using stable isotopologues of water vapor, *J. Atmos. Sci.*, *72*, 2055–2069.

Garreaud, R. D., and J. M. Wallace (1998), Summertime incursions of midlatitude air into subtropical and tropical South America, *Mon. Weather Rev.*, *126*, 2713–2733.

Garreaud, R. D. (1999), Cold air incursions over subtropical and tropical South America: A numerical case study, *Mon. Weather Rev.*, *127*, 2823–2852.

Garreaud, R. D. (2000), Cold air incursions over subtropical South America: Mean structure and dynamics, *Mon. Weather Rev.*, *128*, 2544–2559.

Garreaud, R. D. (2001), Subtropical cold surges: Regional aspects and global distribution, *Int. J. Climatol.*, *21*, 1181–1197.

Gkinis, V., S. Simonsen, S. Buchardt, J. White, and B. Vinther (2014), Water isotope diffusion rates from the NorthGRIP ice core for the last 16,000 years glaciological and paleoclimatic implications, *Earth Planet. Sci. Lett.*, *405*, 132–141.

Gonçalves, F. L. T., P. L. Silva Dias, and G. P. Araújo (2002), Climatological analysis of wintertime extreme low temperatures in São Paulo City, Brazil: Impact of sea-surface temperature anomalies, *Int. J. Climatol.*, *22*, 1511–1526.

Grootes, P. M., M. Stuiver, L. G. Thompson, and E. Mosley-Thompson (1989), Oxygen isotope changes in tropical ice, Quelccaya, Peru, *J. Geophys. Res.*, *94*(D1), 1187–1194.

Hoffman, G., et al. (2003), Coherent isotope history of Andean ice cores over the last century, *Geophys. Res. Lett.*, *30*(4), 1179, doi:10.1029/2002GL014870.

Hurley, J. V., M. Vuille, D. R. Hardy, S. J. Burns, and L. G. Thompson (2015), Cold air incursions, δ^{18}O variability, and monsoon dynamics associated with snow days at Quelccaya Ice Cap, Peru, *J. Geophys. Res. Atmos.*, *120*, 7467–7487, doi:10.1002/2015JD023323.

Li, J., and H. J. Zwally (2011), Modeling of firn compaction for estimating ice-sheet mass change from observed ice-sheet elevation change, *Ann. Glaciol.*, *52*(59), 1–7.

Merlivat, L. (1978), Molecular diffusivities of $H_2^{16}O$, HD^{16}, and $H_2^{18}O$ in gases, *J. Chem. Phys.*, *69*(6), 2864–2871.

Müller, G. V., M. A. Gan, E. Dal Piva, and V. Piccinini Silveira (2015), Energetics of wave propagation leading to cold event in tropical latitudes of South America, *Clim. Dyn.*, *45*, 1–20.

NASA (2015), *Jet Propulsion Laboratory, Aura TES Group, TES Lite Products*. [Available at http://avdc.gsfc.nasa. gov.]

Noone, D. (2012), Pairing measurements of the water vapor isotope ratio with humidity to deduce atmospheric moistening and dehydration in the tropical midtroposphere, *J. Clim.*, *25*, 4476–4494.

Risi, C., S. Bony, and F. Vimeux (2008), Influence of convective processes on the isotopic composition (δ^{18}O and δD) of precipitation and water vapor in the tropics: 2. Physical interpretation of the amount effect, *J. Geophys. Res.*, *117*, D05304, doi:10.1029/2008JD009943.

Risi, C., et al. (2012), Process-evaluation of tropospheric humidity simulated by general circulation models using water vapor isotopologues: 1. Comparison between models and observations, *J. Geophys. Res.*, *117*, D05304, doi:10.1029/2011JD016623.

Rozanski, K., L. Araguás, and R. Gonfiantini (1993), Isotopic patterns in modern global precipitation, in *Climate Change in Continental Isotopic Records, Geophys. Monogr. Ser.*, vol. 78, edited by P. K. Swart, pp. 1–36, AGU, Washington, D. C.

Sachs, H. M., T. Webb III, and D. R. Clark (1977), Paleoecological transfer functions, *Annu. Rev. Earth Planet. Sci.*, *5*, 159–178.

Samuels-Crow, K., J. Galewsky, D. R. Hardy, Z. D. Sharp, J. Worden, and C. Braun (2014), Upwind convective influences on the isotopic composition of atmospheric water vapor over the tropical Andes, *J. Geophys. Res. Atmos.*, *119*, 7051–7063, doi:10.1002/2014JD021487.

Sjolte, J., G. Hoffman, S. J. Johnsen, B. M. Vinther, V. Masson-Delmotte, and C. Sturm (2011), Modeling the water isotopes in Greenland precipitation 1959–2001 with the meso-scale model REMO-iso, *J. Geophys. Res.*, *116*, D18105, doi:10.1029/2010JD015287.

Steen-Larsen, H. C., et al. (2011), Understanding the climatic signal in the water stable isotope records from the NEEM shallow firn/ice cores in northwest Greenland, *J. Geophys. Res.*, *116*, D06108, doi:10.1029/2010JD014311.

Stichler, W., U. Schotterer, K. Fröhlich, P. Ginot, C. Kull, H. Gäggeler, and B. Pouyaud (2001), Influence of sublimation on stable isotope records recovered from high-altitude glaciers in the tropical Andes, *J. Geophys. Res.*, *106*(D19), 22,613–22,620.

Sturm, C., Q. Zhang, and D. Noone (2010), An introduction to stable water isotopes in climate models: Benefits of forward proxy modelling for paleoclimatology, *Clim. Past*, *6*, 115–129.

Thompson, D. M., T. R. Ault, M. N. Evans, J. E. Cole, and J. Emile-Geay (2011), Comparison of observed and simulated tropical climate trends using a forward model of coral δ^{18}O, *Geophys. Res. Lett.*, *38*, L14706, doi:10.1029/2011GL048224.

Thompson, L. G. (1980), Glaciological investigations of the tropical Quelccaya Ice Cap, Peru, *J. Glaciol.*, *25*(91), 69–84.

Thompson, L. G., and W. Dansgaard (1975), Oxygen isotope and microparticle studies of snow samples from Quelccaya Ice Cap, Peru, *Antarct. J. U. S.*, *10*(1), 24–26.

Thompson, L. G., E. Mosley-Thompson, J. F. Bolzan, and B. R. Koci (1985), A 1500-year record of tropical precipitation in ice cores from the Quelccaya Ice Cap, Peru, *Science*, *229*, 971–973.

Thompson, L. G., E. Mosley-Thompson, M. Davis, P. N. Lin, T. Yao, M. Dyurgerov, and J. Dai (1993), Recent warming: Ice core evidence from tropical ice cores with emphasis on central Asia, *Global Planet. Change*, *7*, 145–156.

Thompson, L. G., E. Mosley-Thompson, M. E. Davis, V. S. Zagarodnov, I. M. Howat, V. N. Mikhalenko, and P. N. Lin (2013), Annually resolved ice core records of tropical climate variability over the past 1800 years, *Science*, *340*, 945–950.

Tierney, J. E., S. C. Lewis, B. I. Cook, A. N. LeGrande, and G. Schmidt (2011), Model, proxy, and isotopic perspectives on the East African Humid Period, *Earth. Planet. Sci. Lett.*, *307*(1–2), 103–112.

Tindall, J. C., P. J. Valdes, and L. C. Sime (2009), Stable water isotopes in HadCM3: Isotopic signature of El Niño–Southern Oscillation and the tropical amount effect, *J. Geophys. Res.*, *114*, D04111, doi:10.1029/2008JD010825.

Tingley, M. P., P. F. Craigmile, M. Haran, B. Li, E. Mannshardt, and B. Rajaratnam (2012), Piecing together the past: Statistical insights into paleoclimatic reconstructions, *Quat. Sci. Rev.*, *35*, 1–22.

van der Wel, G., H. Fischer, H. Oerter, H. Meyer, and H. A. J. Meijer (2015), Estimation and calibration of the water isotope differential diffusion length in ice core records, *Cryosphere*, *9*, 1601–1616.

Vimeux, F., P. Ginot, M. Schwikowski, M. Vuille, G. Hoffman, L. G. Thompson, and U. Schotterer (2009), Climate variability during the last 1000 years inferred from Andean ice cores: A review of methodology and recent results, *Palaeogeogr. Palaeoclimatol. Palaeoecol.*, *281*, 229–241.

Vuille, M., R. S. Bradley, M. Werner, R. Healy, and F. Keimig (2003a), Modeling δ^{18}O in precipitation over the tropical Americas: 1. Interannual variability and climatic controls, *J. Geophys. Res.*, *108*(D6), 4174, doi:10.1029/2001JD002038.

Vuille, M., R. S. Bradley, R. Healy, M. Werner, D. R. Hardy, L. G. Thompson, and F. Keimig (2003b), Modeling $\delta^{18}O$ in precipitation over the tropical Americas: 2. Simulation of the stable isotope signal in Andean ice cores, *J. Geophys. Res.*, *108*(D6), 4175, doi:10.1029/2001JD002039.

Vuille, M., and M. Werner (2005), Stable isotope in precipitation recording South American summer monsoon and ENSO variability: Observations and model results, *Clim. Dyn.*, *25*, 401–413.

Vuille, M., S. J. Burns, B. L. Taylor, F. W. Cruz, B. W. Bird, M. B. Abbott, L. C. Kanner, H. Cheng, and V. F. Novello (2012), A review of the South American monsoon history as recorded in stable isotopic proxies over the past two millenia, *Clim. Past*, *8*, 1309–1321.

Worden, J., et al. (2006), Tropospheric Emission Spectrometer observations of the tropospheric HDO/H_2O ratio: Estimation approach and characterization, *J. Geophys. Res.*, *111*, D16309, doi:10.1029/2005JD006606.

Worden, J., D. Noone, J. Galewsky, A. Bailey, K. Bowman, D. Brown, J. Hurley, S. Kulawik, J. Lee, and M. Strong (2011), Estimate of bias in Aura TES HDO/H_2O profiles from comparison of TES and in situ HDO/H_2O measurements at the Mauna Loa Observatory, *Atmos. Chem. Phys.*, *11*, 4491–4503.

Worden, J., S. Kulawik, C. Frankenberg, V. Payne, K. Bowman, K. Cady-Peirara, K. Wecht, and J.-E. Lee (2012), Profiles of CH_4, HDO, H_2O, and N_2O with improved lower tropospheric vertical resolution from Aura TES radiances, *Atmos. Meas. Tech.*, *5*, 397–411.

Erratum

In the originally published version of this article, per mil symbols were incorrectly typeset as (‰0). The error has since been corrected, and this version may be considered the authoritative version of record.